Predissociation dynamics of the $A^2\Sigma^+$ state of SH radical: Fine-structure state distributions of the $S(^3P_J)$ products

Yuan Qin, Xianfeng Zheng[a], Yu Song[b], Ge Sun[c], and Jingsong Zhang*

Department of Chemistry

University of California at Riverside

Riverside, California 92521

U.S.A.

Abstract

Photo-predissociation of rovibrational levels of SH ($A^2\Sigma^+$, v' = 0-6) is studied using the high-n Rydberg atom time-of-flight technique. Spin-orbit branching fractions of the $S(^3P_{J=2,1,0})$ products are measured in the product translational energy distributions. The SH $A^2\Sigma^+$ v' = 0 state predissociates predominantly via coupling to the $^4\Sigma^-$ repulsive state. As the vibrational level v' increases, predissociation dynamics change drastically, with all three repulsive states ($^4\Sigma^-$, $^2\Sigma^-$, and $^4\Pi$) involved in the dissociation. Nonadiabatic interactions and quantum interferences among these dissociation pathways affect the fine-structure state distributions of the $S(^3P_{J=2,1,0})$ products.

a. Permanent address: Department of Physics, Anhui Normal University, Wuhu, Anhui 241000, P. R. China.

b. Permanent address: Beijing Academy of Quantum Information Sciences, Beijing, 100193, P. R. China.

c. Present address: Dalian Institute of Chemical Physics, Chinese Academy of Sciences, Dalian, Liaoning 116023, P. R. China.

* Corresponding author. E-mail: jingsong.zhang@ucr.edu. Fax: 1-951-827-4713. Also at the Air Pollution Research Center, University of California, Riverside, CA 92521, USA.

SH radical is a prototypical diatomic system for studying photodissociation and nonadiabatic dynamics of open-shell electronic excited states. Its low-lying excited states are readily accessible and the atomic photofragments can be precisely characterized experimentally, while full quantum theory on the photodissociation properties of this small system is feasible and can be compared with the experimental observations at high levels.

The electronic states of SH have been extensively examined by theory[1-8] and experiments.[9-17] The ground state $X^2\Pi$ of SH adiabatically correlates with atomic products $H(^2S) + S(^3P_J)$ (Figure 1). Optically coupled to the ground $X^2\Pi$ state, the first excited state, $A^2\Sigma^+$, correlates with $H(^2S) + S(^1D)$ in the atomic limit. The $A^2\Sigma^+$ state is crossed by three repulsive states ($^4\Sigma^-$, $^2\Sigma^-$, and $^4\Pi$) in the Franck-Condon (FC) region, which all correlate with $H(^2S) + S(^3P_J)$. The spectroscopy of the SH $A^2\Sigma^+ - X^2\Pi$ band has been well studied,[9-11,18-21] and the diffuse spectra reaching the $A^2\Sigma^+$ $v' \geq 1$ levels indicate occurrence of rapid predissociation. The predissociation of the $A^2\Sigma^+$ state is induced by spin-orbit couplings with the repulsive $^4\Sigma^-$, $^2\Sigma^-$, and $^4\Pi$ states. Depending on the positions where curves cross in the FC region, the $A^2\Sigma^+$ v' = 0-1 levels predissociate mainly through the $^4\Sigma^-$ state; at v' = 2-3, the three repulsive states make significant contributions to the dissociation process; and for the higher v' = 4-6 levels, the $^4\Pi$ state has a dominant involvement.[6,17] The predissociation lifetime of SH $A^2\Sigma^+$ is ~ 0.17-3 ns for v' = 0,[11,12,22] and it is on the order of picosecond for $v' \geq 1$ as they are closer to the crossing points.[17,21] Outside the crossing points and at larger internuclear separations (recoupling region) where the spin-orbit interactions are comparable to the electronic energy separations, intrastate couplings among the three repulsive states can redistribute the dissociative flux among the involving states.[23-25] At asymptotical region, the spin-orbit interactions (through transformation from molecular states to atomic terms) could also affect the $S(^3P_J)$ fine-structure state distributions.[23-25]

Compared with OH radical, reports on the predissociation dynamics of SH are fewer. Lee and co-workers analyzed the predissociation process of the SH $A^2\Sigma^+$ state with quantum scattering calculations.[23] At the $N' = 12$ level of the $A^2\Sigma^+$ $v' = 0$ state, the S($^3P_{J=2,1,0}$) branching fractions were predicted to be 0.910:0.031:0.059, and the influence of the splitting of the F_1 and F_2 components was minimal. While at higher energies, for instance, $v' = 6$ and $N' = 6$, the contribution from the direct dissociation via the $^2\Sigma^-$ state would increase and result in slow variation in the branching ratios across the resonance. The computed branching ratios for the $v' = 0$ and 6 states are distinct from single-state diabatic limit (assuming that the dissociation occurs suddenly on a single repulsive state), indicating strong intrastate couplings in this energy region. Experimentally, Parker and co-workers investigated the predissociation of SH and SD $A^2\Sigma^+$ ($v' = 0$-2) using velocity map imaging.[26] For SH $A^2\Sigma^+$ $v' = 0$, the S($^3P_{J=2,1,0}$) branching ratios were determined to be $0.80^{+0.09}_{-0.10}$: $0.07^{+0.07}_{-0.03}$:$0.13^{+0.10}_{-0.09}$. The dominant S($^3P_2$) product suggests that predissociation of $A^2\Sigma^+$ $v' = 0$ is mainly through the $^4\Sigma^-_{1/2}$ state, followed by spin-orbit couplings among the three repulsive states at large internuclear separations. For SH $A^2\Sigma^+$ $v' = 1$ and 2, the measured branching fractions of S($^3P_{J=2,1,0}$) were $0.76^{+0.06}_{-0.08}:0.06^{+0.06}_{-0.02}:0.18^{+0.07}_{-0.04}$ and $0.62^{+0.04}_{-0.08}:0.04^{+0.06}_{-0.02}:0.34^{+0.07}_{-0.05}$, respectively. The increased branching of S($^3P_0$) is consistent with the contribution from the $^2\Sigma^-$ and $^4\Pi$ states. And the S($^3P_2$) $m_s = \pm 2$ products exhibited little population, indicating weak or negligible Coriolis couplings during the dissociation.

In this work, we report a study on the predissociation of SH $A^2\Sigma^+$ $v' = 0$-6, which is similar to our previous work on OH $A^2\Sigma^+$ $v' = 2$-4.[27,28] With the high-resolution technique, the initial quantum state of SH was well specified in the photoexcitation, and the S(^3P_J) product fine-structure states from different vibrational levels of $A^2\Sigma^+$ were all resolved and measured. Results for SH in this work are compared with the previous results for the analogous OH radical. This work explores

the predissociation dynamics of the SH $A^2\Sigma^+$ state and the nonadiabatic interactions along the dissociation coordinate, from the FC region to the recoupling zone and the asymptotic region.

The experimental apparatus and high-*n* Rydberg atom time-of-flight (HRTOF) method have been reported previously.[27-30] The SH radicals were prepared by photolyzing H_2S precursors (≥ 99.5%, Aldrich; ~ 6% in Ar at ~ 120 kPa) at the exit of a pulsed nozzle with 193-nm ArF excimer laser radiation. The SH radicals were entrapped and cooled in a supersonic beam. The radicals in the beam entered the main chamber through a skimmer and were crossed and photodissociated by a near-ultraviolet laser radiation (280-333 nm, ~ 0.3 cm^{-1} linewidth, 5-12 mJ/pulse, and linearly polarized). The absolute photodissociation wavelength was measured by a Burleigh wavemeter. The photodissociation laser polarization was adjusted by an achromatic λ/2 plate for measurements of product angular distributions. The SH radicals in the beam had a rotational temperature of ~ 45 K, estimated by assuming a rotational population at thermal equilibrium. At this temperature, the ground state $X^2\Pi_{3/2}$ (v'' = 0, N'' = 1, J'' = 1.5, F_1) was mainly populated (~ 68%). Specific rovibrational states of SH $A^2\Sigma^+$ (v' = 0-2) were reached by positioning the photodissociation wavelength precisely at the wavelengths of the known SH transitions [$A^2\Sigma^+$ (v' = 0-2, N', J', F_1) ← $X^2\Pi$ (v'' = 0-1, N'', J'', F_1)].[9,10] The rotational states of higher vibrational levels of SH $A^2\Sigma^+$ (v' = 3-6) were reached by scanning the laser around the $A^2\Sigma^+$ (v' = 3-6) ← $X^2\Pi$ (v'' = 0-2) bands, which were predicated with the spectroscopic constants[5,14,31] and analyzed in our recent work.[21] The H-atom photoproducts were excited by two-color resonant excitation (121.6 nm + 366.2 nm) to a metastable high-*n* Rydberg state (n ~ 30). A small portion of the neutral Rydberg H atoms drifted toward a microchannel plate detector and were detected after field ionization. The flight length was 37.27 cm, calibrated by using energetics of the two-photon photodissociation products $H(^2S) + S(^1D)$ and $H(^2S) + S(^1S)$ and the one-photon photodissociation

products $H(^2S) + S(^3P_J)$.[32] The H-atom TOF spectra were accumulated typically with ~ 20-80 k laser shots.

The H-atom TOF spectra at the SH $A^2\Sigma^+$ (v' = 0-6) ← $X^2\Pi$ (v'' = 0-2) transitions showed several sharp peaks and a small broad background. Specifically, the SH $A^2\Sigma^+$–$X^2\Pi$ (v', v'') bands investigated include (a,0) (a = 0-3), (b,1) (b = 1-2 and 4), and (c,2) (c = 4-6). The weak broad background, still present when the 193-nm laser for radical production was turned off, was from the precursors. When the photodissociation laser wavelength was tuned off the SH $A^2\Sigma^+ \leftarrow X^2\Pi$ transitions (by several cm^{-1}), the intense sharp peaks vanished and the small broad background was essentially identical to the precursor background. This broad background was properly removed for the net H-atom TOF spectra from photodissociation of SH. Some minor sharp peaks remained in certain off-resonance spectra, which were attributed to the H + $S(^3P_J)$ products of direct photodissociation of SH from the repulsive $^2\Sigma^-$ state (excited from $X^2\Pi$ v'' = 2-4), or the H + $S(^1D)$ products from the repulsive wall of the $A^2\Sigma^+$ state (excited from $X^2\Pi$ v'' = 3-5).[32,33] With the large energy spacing between the vibrational levels, the H-atom signals from different vibrational levels of $X^2\Pi$ were well separated. Due to the much smaller FC factors, there was little or no contribution from transitions of $^2\Sigma^- \leftarrow X^2\Pi$ (v'' = 2) at the wavelengths of the SH $A^2\Sigma^+$ (v' = 4-6) ← $X^2\Pi$ (v'' = 2) bands. The H-atom photofragment yield (PFY) spectra of the SH $A^2\Sigma^+$ (v' = 0-6) ← $X^2\Pi$ (v'' = 0-2) transitions were constructed by integrating the intensities of the intense sharp peaks in the net H-atom TOF spectra versus photodissociation wavelengths across the transition resonances.[21] The PFY spectra reproduced the SH $A^2\Sigma^+$ (v' = 0-2) ← $X^2\Pi$ (v'' = 0) absorption lines in literature.[9,10,21] The intensities of the sharp peaks in the TOF spectra depended linearly on the photodissociation laser power, and their flight times and corresponding product kinetic energies agreed well with the SH bond dissociation energy.[29,32] These observations

definitely confirmed predissociation of the SH $A^2\Sigma^+$ (v' = 0-6) states as the origin of the intense sharp peaks in the TOF spectra. The minor contributions from direct dissociation of the repulsive states ($^2\Sigma^-$ and repulsive part of $A^2\Sigma^+$) were well separated and can be readily removed in the studied wavelength regions.

To prepare the rovibronic level of the $A^2\Sigma^+$ state (v' = 0-6, N' = 0), $P_1(1.5)$ transition was used (or near it for the rotationally unsolved v' = 3-6 levels), i.e. $A^2\Sigma^+$ (v' = 0-6, N' = 0, J' = 0.5) ← $X^2\Pi$ (v'' = 0-2, N'' = 1, J'' = 1.5). The net H-atom TOF spectra via the $P_1(1.5)$ transition were measured with the photodissociation laser polarization perpendicular ($\theta = 90°$), at magic angle ($\theta = 54.7°$), and parallel ($\theta = 0°$) with the TOF path (direction of detection), respectively. Figure 2 shows a representative center-of-mass (CM) product translational energy distribution, $P(E_T)$, converted from the H-atom TOF spectrum of SH predissociation at magic angle via the $A^2\Sigma^+$–$X^2\Pi$ (0, 0) $P_1(1.5)$ transition at 30832.68 cm^{-1}. The three peaks in the $P(E_T)$ are from the three H(^{2}S) + S($^3P_{J=2,1,0}$) product channels. The magic angle $P(E_T)$ is independent of the anisotropy parameter and is proportional to angle-integrated $P(E_T)$, thus it is utilized to evaluate branching ratios of the different product channels.

To extract the S($^3P_{J=2,1,0}$) product fine-structure state populations, the $P(E_T)$'s are deconvoluted using three slightly asymmetric double Gaussian peaks (as instrumentation function). The ground-state S($^3P_2$) peak, with recognizable intensity and well separated, is fitted first to establish the line shape. The S($^3P_1$) and S($^3P_0$) peaks are deconvoluted, with the same line shape and their positions fixed relative to S($^3P_2$) [with spin-orbit energy splitting: S($^3P_2$), 0.0 cm^{-1}; S($^3P_1$), 396.1 cm^{-1}; S($^3P_0$), 573.6 cm^{-1}].[34] As only the peak heights are adjusted, the deconvolution is robust (see Figure 2). Due to the relatively small rotational constants and broad linewidth, there are small contributions from other initial rotational states of the ground state $X^2\Pi$ (N'') in some

transitions. For instance, in the $P(E_T)$ from the SH (1,0) $P_1(1.5)$ transition, the minor peaks near major ones result from another transition starting at $X^2\Pi$ (v'' = 0, N'' = 2, J'' = 2.5, F_1) [near $Q_1(2.5)$ resonance]. These overlapping transitions in v' = 0-2 are carefully treated, with similar peak fitting and the minor peak positions relative to the main ones fixed at the rotational energy spacing of the $X^2\Pi$ state. Whilst for $v' \geq 3$ levels, the peaks in $P(E_T)$'s are much broader, the minor contributions from other rotational N'' levels of the $X^2\Pi$ state were unsolved. For comparison, relative intensities and best fits of the three $S(^3P_J)$ product peaks in predissociation of SH ($A^2\Sigma^+$, v' = 0-6) via the $P_1(1.5)$ transition (or near this) at magic angle are presented in Figure 3 by replotting the magic angle $P(E_T)$'s versus the spin-orbit energy of $S(^3P_J)$. The relative peak areas in the best fits of the magic angle $P(E_T)$'s provide spin-orbit branching fractions of the $S(^3P_J)$ products as shown in Figure 4, which reveal significant variation from $A^2\Sigma^+$ v' = 0 to 6. The $S(^3P_J)$ product fine-structure state populations from the predissociation of SH ($A^2\Sigma^+$, v' = 0-6) via the $P_1(1.5)$ transitions (or near this) are listed in Table I, where the $A^2\Sigma^+$ (v' = 1-2 and 4) states were reached by transitions starting from various initial vibrational levels of $X^2\Pi$ (v'' = 0-2). Even with different initial states (v''), these transitions produced similar branching fractions within the error limits when reaching the same $A^2\Sigma^+$ vibrational level (v'). The branching ratios of the SH $A^2\Sigma^+$ (v' = 0-2) ← $X^2\Pi$ (v'' = 0) $P_1(1.5)$ transitions agree within the error limits with those by Parker and co-workers,[26] although our results indicate somewhat higher population for the $S(^3P_2)$ product and lower for $S(^3P_0)$.

Analogous to the OH radical, the predissociation dynamics of the $A^2\Sigma^+$ state and the $S(^3P_J)$ product fine-structure state distributions depend on the initial rovibrational levels of the $A^2\Sigma^+$ state, which determine the initial dissociative flux from $A^2\Sigma^+$ to the three repulsive states via spin-orbit couplings in the crossing region, the predissociation time scale, and the kinetic energy of the products (thus the transverse time along the repulsive curves).[23-25,35] The $S(^3P_J)$ fine-structure state

distributions are further influenced by spin-orbit and Coriolis couplings among the $^4\Sigma^-$, $^2\Sigma^-$, and $^4\Pi$ states [the S(^3P_J) intrashell interactions] at larger internuclear distance (the recoupling region), and finally asymptotic spin-orbit interactions at the largest internuclear distances.[23-25,35] With similar potential energy curves (PECs), the predissociation dynamics of SH $A^2\Sigma^+$ should be close to those of OH, although the spin-orbit energy splitting in S(^3P_J) are larger and the excited electronic and vibrational energies of SH $A^2\Sigma^+$ are lower (thus lower product kinetic energies).

As the v' = 0 and 1 levels lie far below the lowest crossing of $A^2\Sigma^+$ and $^4\Sigma^-$, the predissociation is mostly via the $^4\Sigma^-$ state.[6,17,23,26] According to the Fermi golden rule calculations by Brite et al., the contributions from the repulsive states to the predissociation rates are $^4\Sigma^-$ (100.0%), $^2\Sigma^-$ (0.0%), and $^4\Pi$ (0.0%) for v' = 0 and $^4\Sigma^-$ (99.7%), $^2\Sigma^-$ (0.3%), and $^4\Pi$ (0.0%) for v' = 1.[6] In the adiabatic limit, when the dissociation slowly follows the PEC of $^4\Sigma^-$ the S($^3P_{J=2,1,0}$) product branching fractions would be 1:0:0.[23,26] While the sudden (diabatic) limit from $^4\Sigma^-$ gives the S($^3P_{J=2,1,0}$) branching ratios of 0.611:0.167:0.222 by projecting the molecular wavefunction of $^4\Sigma^-$ to the S($^3P_{J=2,1,0}$) atomic basis set, ignoring the intrashell interactions and asymptotic spin-orbit couplings.[23,25,35] The experimental results for v' = 0 and 1 are closer to the adiabatic limit than the diabatic limit, consistent with the dominant role of $^4\Sigma^-$ among the three repulsive states and a slow dissociation on $^4\Sigma^-$. In comparison, the predissociation of lower vibrational state v' = 2 of OH $A^2\Sigma^+$ is close to the diabatic limit.[28] The difference between OH $A^2\Sigma^+$ v' = 2 and SH $A^2\Sigma^+$ v' = 0-1 can be explained by the adiabaticity parameter: $\varepsilon = \frac{R}{v} \cdot \frac{\Delta E}{\hbar}$, where v is the recoil velocity, R the length of interaction region, and ΔE is the energy separation of the interacting states. With the larger spin-orbit splitting of the S(^3P_J) atomic products and smaller product kinetic energy, the adiabaticity degree of SH v' = 0-1 is larger by a factor of ~ 3-4 than that of OH v' = 2. The experimental S(^3P_J) product branching ratios of SH $A^2\Sigma^+$ v' = 0-1, however, are not exactly at the adiabatic limit,

showing a small amount of $S(^3P_{1,0})$ products. These evidently indicate that there are nonadiabatic couplings among the three repulsive states at large internuclear distance and a small amount of dissociation flux transfers from $^4\Sigma^-$ to $^2\Sigma^-$ and $^4\Pi$. Indeed, the quantum scattering calculations that treat all the nonadiabatic couplings in the dissociation process predicted the $S(^3P_{J=2,1,0})$ branching fractions to be 0.910:0.031:0.059 for $v' = 0$, $N' = 12$,[23] in excellent agreement with our values for $v' = 0$, $N' = 0$.

As the levels $v' = 2$-3 locate between the crossing points, all three repulsive states are involved in the predissociation process. The relative predissociation rates are calculated to be: $^4\Sigma^-$ (69.8%), $^2\Sigma^-$ (25.5%), and $^4\Pi$ (4.7%) for $v' = 2$ and $^4\Sigma^-$ (15.0%), $^2\Sigma^-$ (36.7%), and $^4\Pi$ (48.3%) for $v' = 3$.[6] With the increased excitation energy and thus product kinetic energy, diabatic (sudden) limit may become preferred to the adiabatic limit. In the sudden limit (by frame transformation), single-state branching ratios are $S(^3P_{J=2,1,0}) = 0.611:0.167:0.222$ for $^4\Sigma^-$, 0.556:0.333:0.111 for $^2\Sigma^-$, and 0.306:0.250:0.444 for $^4\Pi$, respectively.[23,25,35] In a noncoherent average approximation, the $S(^3P_J)$ spin-orbit branching ratios is modelled by combining the sudden-limit single-state $S(^3P_J)$ spin-orbit branching ratios with weightage of the square root of the corresponding single-state predissociation rates of the three repulsive states, while neglecting the spin-orbit and Coriolis interactions in the recoupling zone and the interferences among the repulsive states in the asymptotic region.[6,25] The product branching ratios are predicted to be $S(^3P_{J=2,1,0}) = 0.551:0.232:0.217$ for $v' = 2$, and 0.465:0.261:0.274 for $v' = 3$. The experimental $S(^3P_J)$ branching ratios for $A^2\Sigma^+$ ($v' = 2$-3, $N' = 0$) do not match the noncoherent average predications. The failure of the simple noncoherent average approximation suggests that the interactions and interferences among the three repulsive states in the recoupling zone and/or the asymptotic region are non-negligible. It is expected that in addition to the nonadiabatic interactions among the repulsive $^4\Sigma^-$,

$^2\Sigma^-$, and $^4\Pi$ dissociative pathways there are quantum interferences among them in the recoupling zone and asymptotic region, as the predissociation is initiated coherently from the same bound state of $A^2\Sigma^+$ and proceeds to the final $S(^3P_J)$ products with several indistinguishable pathways. In fact, the quantum interferences were clearly observed in the predissociation of OH $A^2\Sigma^+$ $v' = 4$, where all three repulsive states contribute and the final spin-orbit branching fractions of the $O(^3P_J)$ products are strongly influenced.[27,28] For higher levels $v' \geq 4$, although the $^4\Pi$ state is the nearest repulsive state, the single-state approximation of $^4\Pi$ is inadequate to interpret the experimental branching ratios. The difference between the noncoherent average predictions and the experimental results is even more significant. This again indicates very strong interstate inferences among the dissociation channels at these higher energies. However, the full quantum calculations of the branching ratios for $v' = 6$ and $N' = 6$ by Lee and coworkers predicted $S(^3P_{J=2,1,0})$ = 0.003:0.877:0.120 (which may also be influenced by additional direct dissociation via the $^2\Sigma^-$ state),[23] in significant disagreement with our experimental measurements for $v' = 6$. This signifies the challenges to accurately account for all the nonadiabatic interactions and quantum interferences in the multiple pathway predissociation of the SH $A^2\Sigma^+$ state, especially from the higher vibrational levels.

In closing, the $S(^3P_J)$ product spin-orbit branching fractions from predissociation of the SH $A^2\Sigma^+$ ($v' = 0$-6, $N' \approx 0$) states are completely measured for the first time. As the vibrational level v' increases, contributions of the three repulsive states to the predissociation of $A^2\Sigma^+$ increases from $^4\Sigma^-$ only (for $v' = 0$) to all $^4\Sigma^-$, $^2\Sigma^-$, and $^4\Pi$ (for $v' = 1$-6). The $S(^3P_J)$ product spin-orbit branching fractions are strongly influenced by the nonadiabatic interactions and quantum interferences among the multiple dissociation pathways. The experimental results provide benchmarks for full

quantum theory that accurately and completely describes the complex predissociation dynamics of the SH $A^2\Sigma^+$ state.

This work was supported by the US National Science Foundation (Grant No. CHE-2155232). Y. Qin acknowledges support from a UC Riverside Dissertation-Year Fellowship. X. Zheng acknowledges partial support from the University Annual Scientific Research Plan of Anhui Province (Grant No. 2022AH010013). We thank Profs. Millard Alexander, Paul Dagdigian, and Richard Dawes for helpful discussions.

Conflict of interest

The authors have no conflicts to disclose.

References

1. D. M. Hirst and M. F. Guest, *Molecular Physics* **46**, 427 (1982).
2. P. J. Bruna and G. Hirsch, *Molecular Physics* **61**, 1359 (1987).
3. J. K. Park and H. Sun, *Chemical physics letters* **194**, 485 (1992).
4. M. R. Manaa, *International Journal of Quantum Chemistry* **56**, 577 (1995).
5. S. M. Resende and F. R. Ornellas, *The Journal of chemical physics* **115**, 2178 (2001).
6. V. Brites, D. Hammoutène, and M. Hochlaf, *Journal of Physics B: Atomic, Molecular and Optical Physics* **41**, 045101 (2008).
7. B. S. D. R. Vamhindi and M. Nsangou, *Molecular Physics* **114**, 2204 (2016).

8. S.-T. Zhao, X.-P. Liu, R. Li, H.-J. Guo, and B. Yan, *Chinese Physics B* **30**, 073104 (2021).
9. D. A. Ramsay, *The Journal of Chemical Physics* **20**, 1920 (1952).
10. J. Johns and D. A. Ramsay, *Canadian Journal of Physics* **39**, 210 (1961).
11. W. Ubachs, J. Ter Meulen, and A. Dymanus, *Chemical physics letters* **101**, 1 (1983).
12. R. R. Friedl, W. H. Brune, and J. G. Anderson, *The Journal of chemical physics* **79**, 4227 (1983).
13. J. Tiee, M. Ferris, and F. Wampler, *The Journal of Chemical Physics* **79**, 130 (1983).
14. L. Schnieder, W. Meier, K. Welge, M. Ashfold, and C. Western, *The Journal of Chemical Physics* **92**, 7027 (1990).
15. S. H. Ashworth and J. M. Brown, *Journal of Molecular Spectroscopy* **153**, 41 (1992).
16. E. Klisch, T. Klaus, S. Belov, A. Dolgner, R. Schieder, G. Winnewisser, and E. Herbst, *The Astrophysical Journal* **473**, 1118 (1996).
17. M. D. Wheeler, A. J. Orr-Ewing, and M. N. Ashfold, *The Journal of chemical physics* **107**, 7591 (1997).
18. M. N. Lewis and J. U. White, *Physical Review* **55**, 894 (1939).
19. C. Pathak and H. Palmer, *Journal of Molecular Spectroscopy* **32**, 157 (1969).
20. M. N. Gorman, S. N. Yurchenko, and J. Tennyson, *Monthly Notices of the Royal Astronomical Society* **490**, 1652 (2019).
21. Y. Qin, X. Zheng, Y. Song, G. Sun, and J. Zhang, *The Journal of Chemical Physics* **157**, 134303 (2022).
22. G. W. Loge and J. Tiee, *The Journal of chemical physics* **89**, 7167 (1988).

23. S. Lee, H. Sun, B. Kim, and K. F. Freed, *The Journal of Chemical Physics* **114**, 5537 (2001).

24. D. R. Yarkony, *The Journal of chemical physics* **97**, 1838 (1992).

25. G. Parlant and D. R. Yarkony, *The Journal of chemical physics* **110**, 363 (1999).

26. R. Rose, A. Orr-Ewing, C.-H. Yang, K. Vidma, G. Groenenboom, and D. Parker, *The Journal of chemical physics* **130**, 034307 (2009).

27. W. Zhou, Y. Yuan, and J. Zhang, *The Journal of chemical physics* **119**, 9989 (2003).

28. G. Sun, W. Zhou, X. Zheng, Y. Qin, Y. Song, Y. Yuan, and J. Zhang, *Molecular Physics* **119**, e1837974 (2021).

29. W. Zhou, Y. Yuan, S. Chen, and J. Zhang, *The Journal of chemical physics* **123**, 054330 (2005).

30. X. Zheng, J. Wu, Y. Song, and J. Zhang, *Physical Chemistry Chemical Physics* **11**, 4761 (2009).

31. S. Lee and H. Sun, *Bulletin of the Korean Chemical Society* **22**, 210 (2001).

32. Y. Qin, X. Zheng, Y. Song, G. Sun, and J. Zhang, *Physical Chemistry Chemical Physics* **24**, 27232 (2022).

33. L. M. Janssen, M. P. Van Der Loo, G. C. Groenenboom, S.-M. Wu, D. Č. Radenović, A. J. van Roij, I. A. Garcia, and D. H. Parker, *The Journal of chemical physics* **126**, 094304 (2007).

34. A. Kramida, Yu. Ralchenko, J. Reader, and NIST ASD Team (2021), in *NIST Atomic Spectra Database (ver. 5.9) [Online]* (National Institute of Standards and Technology, Gaithersburg, MD, Available: https://physics.nist.gov/asd [accessed 2022 Jul 17]).

35. Y. Li and P.-Y. Zhang, *J. Theor. Comput. Chem.* **10**, 747 (2011).

Figures and Captions

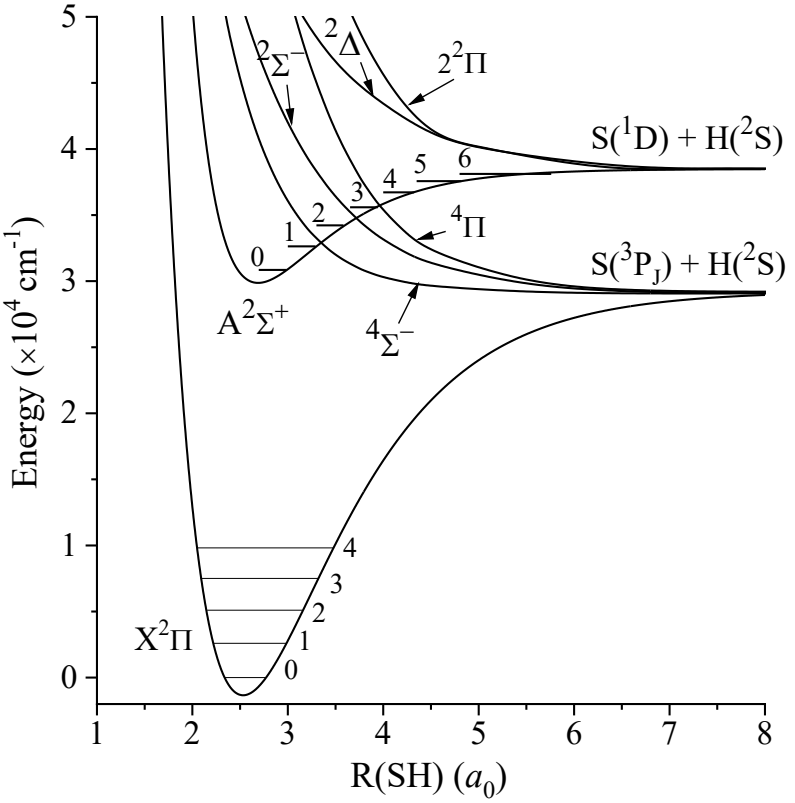

FIG. 1. Potential energy curves of the SH electronic states. The vibrational levels v'' = 0-4 of the $X^2\Pi$ state and v' = 0-6 of the $A^2\Sigma^+$ state are labeled. The information is from Ref 3-5.

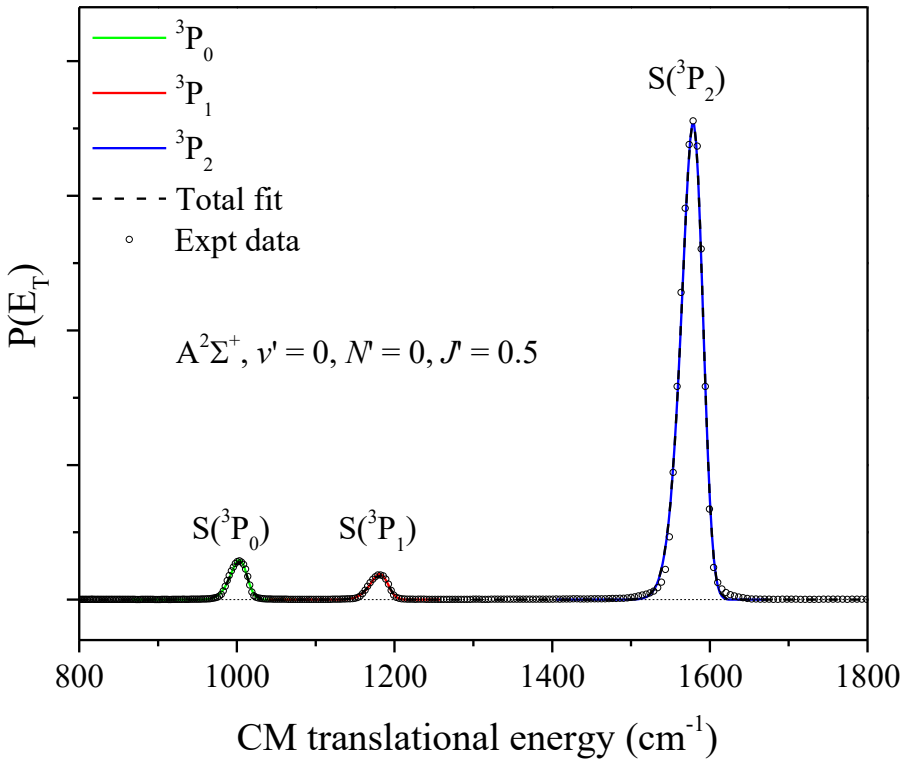

FIG. 2. Center-of-mass translational energy distribution, $P(E_T)$, of $H(^2S) + S(^3P_J)$ products from predissociation of SH ($A^2\Sigma^+$, $v' = 0$, $N' = 0$, $J' = 0.5$, F_1) via the $P_1(1.5)$ transition. The $P(E_T)$ is converted from the net H-atom TOF spectrum with the angle between the polarization of the photodissociation radiation and the TOF path at magic angle $\theta = 54.7°$. The spin-orbit levels of the $S(^3P_{J=2,1,0})$ products are deconvoluted using asymmetric Gaussian peaks (in solid lines). See the text for details.

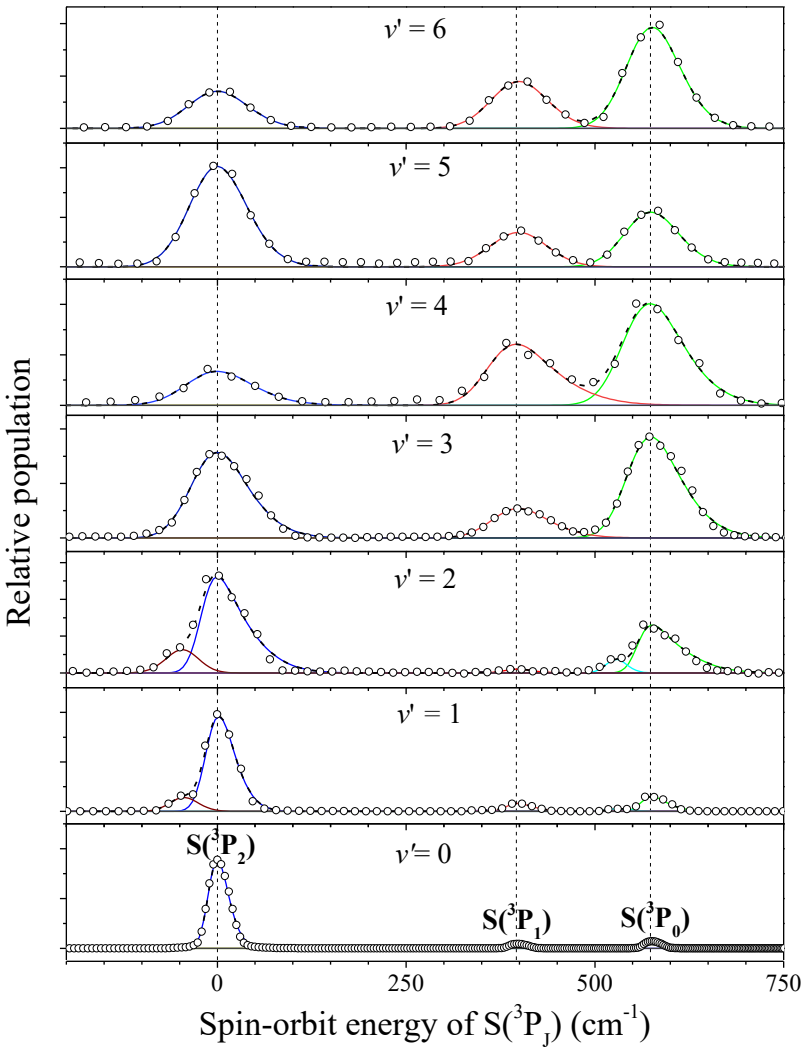

FIG. 3. Relative population of H + $S(^3P_J)$ products as a function of the spin-orbit energy of $S(^3P_J)$, obtained from the magic angle $P(E_T)$'s for the predissociation of SH ($A^2\Sigma^+$, v'= 0-6) via the $P_1(1.5)$ transition (or near that): (0,0) $P_1(1.5)$ at 30832.68 cm^{-1}; (1,0) $P_1(1.5)$ along with $Q_1(2.5)$, $^QP_{21}(2.5)$ (the minor peaks) at 32617.70 cm^{-1}; (2,1) $P_1(1.5)$ along with $Q_1(2.5)$, $^QP_{21}(2.5)$ (the minor peaks) at 31607.19 cm^{-1}; (3,0) at 35575.43 cm^{-1}; (4,2) at 31606.59 cm^{-1}; (5,2) at 32457.99 cm^{-1}; (6,2) at 33013.10 cm^{-1}. The $S(^3P_J)$ product peaks are fitted using asymmetric Gaussian peaks (in solid lines). The peak linewidth was instrumentation function, which increased with increasing product translational energy. Each distribution is scaled to the maximum of its highest peak. See the text for details.

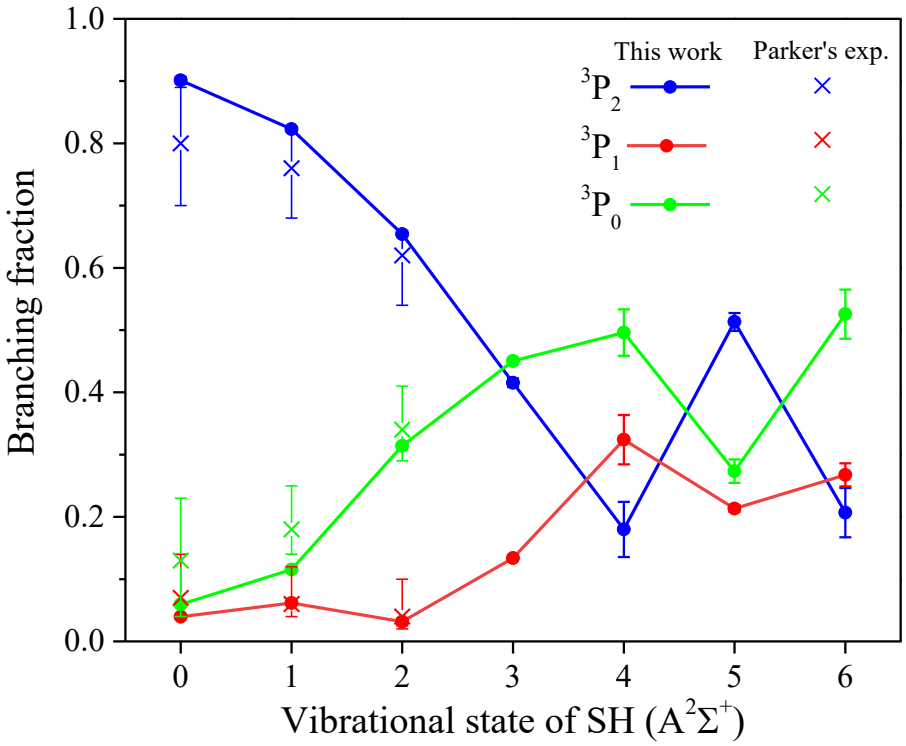

FIG. 4. The fine structure branching fractions of the S($^3P_{J=2,1,0}$) fragments from the predissociation of SH $A^2\Sigma^+$ (v'= 0-6) states. Experimental results in this work (solid circles, derived from FIG. 3), are compared with the measurements from Parker and coworkers (crosses).[26] Error bars in this study represent 95% confidence limit from multiple measurements. The error bars in measurements in Ref 26 were one standard deviation.

TABLE I. Experimental fine-structure state distributions of the $S(^3P_{J=2,1,0})$ fragments from predissociation of SH $A^2\Sigma^+$ (v' = 0-6, N' = 0) states via the $P_1(1.5)$ transition (or near this). The uncertainties (when available) in this study represent 95% confidence limits based on multiple measurements.

Predissociation of SH $A^2\Sigma^+$ (v' = 0-6) ← $X^2\Pi$ (v'' = 0, 1 or 2)					
	Photodissociation $h\nu$ (cm^{-1})		BR_{exp}		
			$^3P_2$	$^3P_1$	$^3P_0$
v' = 0	30832.68	v'' = 0	0.901±0.006	0.040±0.003	0.059±0.004
			[a]$0.80^{+0.09}_{-0.10}$	$0.07^{+0.07}_{-0.03}$	$0.13^{+0.10}_{-0.09}$
			[b]0.910	0.031	0.059
v' = 1	32617.70*	v'' = 0	0.823±0.004	0.062±0.002	0.115±0.003
			[a]$0.76^{+0.06}_{-0.08}$	$0.06^{+0.06}_{-0.02}$	$0.18^{+0.07}_{-0.04}$
	30020.80*	v'' = 1	0.815	0.065	0.120
v' = 2	34206.00*	v'' = 0	0.658±0.002	0.026±0.004	0.316±0.004
			[a]$0.62^{+0.04}_{-0.08}$	$0.04^{+0.06}_{-0.02}$	$0.34^{+0.07}_{-0.05}$
	31607.19*	v'' = 1	0.665±0.013	0.017±0.006	0.318±0.016
v' = 3	35575.43	v'' = 0	0.408±0.010	0.132±0.001	0.460±0.011
v' = 4	34105.55	v'' = 1	0.212	0.282	0.506
	31606.59	v'' = 2	0.180±0.045	0.324±0.040	0.496±0.038
v' = 5	32457.99	v'' = 2	0.522±0.007	0.191±0.006	0.287±0.007
v' = 6	33013.10	v'' = 2	0.230±0.018	0.252±0.025	0.518±0.043

[a]Experimental values from Ref 26. The uncertainties were one standard deviation.

[b]Theoretical value for SH $A^2\Sigma^+$ (v' = 0, N' = 12) from Ref 23.

*Minor contributions from other initial rotational levels J'' are analyzed and removed.